CONF-7811148--2

K_{ID} Values Deduced from Shear Force Measurements on DCB Specimens *

by

C-Lun Chow+ and S.J. Burns

University of Rochester

Rochester, N.Y. 14627

MASTER

* this work was supported by U.S. Dept. of Energy

+ Present address: University of Toronto
Toronto, Canada

DISCLAIMER

Abstract

Time varying shear force measuring techniques have been used to investigate the dynamic critical stress intensity factor versus crack propagation velocity curve. The product of the shear force at the loading end times the square root of the loading time on a rapidly wedged DCB specimen is uniquely related to the critical bending moment at the crack tip. Static compliance measurements on side grooved specimens were incorporated into a Bernoulli-Euler beam model for calibration purposes and to eliminate the inappropriate built-in beam assumption. The compliance calibration shows a crack length shift from a measured crack length to a beam model length at a fixed compliance value. This shift does not effect the magnitude of the calculated critical bending moment at the crack tip when the load and the load point displacement are measured quantities. The effective crack length is calculated from the beam model length with the length shift correction. The K_{ID} values (calculated from the critical bending moment) versus crack velocity have been investigated at several test temperatures for a low carbon steel. K_{ID} values show a generally decreasing trend when crack velocity increases. K_{IC} at fast fracture initiation, is larger than the corresponding K_{ID} value for all tests recorded.

Key words: cantilever beams, crack propagation, fracture properties, critical stress intensity, crack velocity.

Introduction

A series of K_{ID} versus crack velocity data for AISI 1018 cold rolled steel, tested at different temperatures, are presented in this paper. K_{ID} versus crack velocity values are calculated from a directly measurable quantity -- the time varying shear force at the loading end of the rapidly wedged double cantilever beam (DCB) specimen.

The fracture initiates from a sharp starting crack in the DCB specimen with rapid wedge loading. Energy is continuously supplied to the test specimen by the time varying loading force. The slender beam shaped test specimen has a critical bending moment, M*, at the crack tip [1,2]. M* is related to the specific fracture surface energy, R, by $M^* = (RwEI)^{1/2}$, where w is the width of the crack path, E is Young's modulus and I is the moment of inertia of one arm of the beam about the neutral axis. For the constant displacement rate loading DCB, the product of the shear force across the loading end times the square root of the loading time is proportional to M* [3,4]. Therefore, R can be deduced by measuring the time varying shear force across the loading end of a DCB specimen. K_{ID} is assumed to be related to R by a simple static relation, $R = K_{ID}^2/E(1-\nu^2)$, where E is Young's modulus and ν Poisson's ratio.

V-shaped side grooves were machined into all DCB specimens tested in this paper. Because of these grooves, the specimen is softer than beam model predictions. A static compliance measurement incorporated into a Bernoulli-Euler beam model uses a crack length shift at a fixed compliance value. Since $\mathcal{C}$ is proportional to the slope of the compliance versus crack length curve, the length shift correction does not effect the

magnitude of the K value. Therefore, the length shift does not effect the magnitude of the calculated critical bending moment at the crack tip when the load and the load point displacement are the measured quantities. However, crack lengths obtained through beam models must be shift corrected. The time derivative of the crack length gives the crack propagation velocity, $\dot{\ell}$.

In this paper, the test scheme used is briefly described in the first section. Static compliance measurements which lead to corrections to the beam theory are then presented. The K_{ID} versus crack velocity curves are described in the Experimental Results Section. Comparison of K_{IC} and K_{ID} values at the fracture propagation point are then discussed. Finally, general conclusions are summarized.

TEST SCHEME

All the DCB specimens are machined to have the longinitudal direction coincide with the rolling direction of the AISI 1018 cold-rolled steel plate. The DCB specimen, which is designed to be a slender beam and to remain essentially elastic throughout the fracture test, has the nominal dimensions of 2.54 x 5.08 x 42 cm. A more detailed description of the design of the DCB specimens has been reported elsewhere [5,6]. A pair of 60° V-shaped side, crack, guiding grooves were introduced in the thickness direction of each side of the beam. The width of the fractures varies from 0.64 cm to 1.27 cm by increments of approximately 0.32 cm. The fracture is initiated from a short machined starting crack, about 3 cm long, with a swallow-tail cut and fatigued to be totally about 6 cm long. The specimen is fractured by inserting a 30° wedge which is attached to a massive, 300 kg, hammer that free falls from a wedge-drop machine from a height of approximately 2 meters. The energy in the wedge is orders of magnitude larger than the energy in the fracture event. The wedge applies an essentially constant deflection rate of about 1.6 m/sec on each arm of the DCB specimen. The loading machine has been described in detail in ref. [5,6].

A 90° strain gage rosette is mounted, close to the loading point, on the neutral axis of one of the DCB arms. The rosette monitors the time varying shear force across the beam during fracture propagation. The time varying shear force is recorded for calculating K_{ID} versus $\dot{\ell}$ values. The gage and recording instruments used for fracture test is experimentally shown to be adequate for the specified DCB specimen [4].

STATIC COMPLIANCE CALIBRATION

The side grooves for guiding the crack propagation direction have a significant effect of the deformation of the precracked part of the DCB

specimen [4,7,8]. A detailed description of static compliance measurements on the specified fracture specimen is reported in ref. [4]. The measured compliance values at different simulated crack lengths are shown in Fig. 1. The compliance, C, when plotted as $C^{1/3}$ versus the beam length is a straight line as beam models predict, (curve S). Curve (D) is based on the dynamic analysis [2] and the experimentally measured total fracturing time [3] of a specimen with this specified geometry.

The measured compliance value increases monotonically with respect to the simulated crack length, ℓ, and increases rapidly when the crack tip is 1 1/2 beam heights from the free end of the beam. The measured compliance valuesare a reasonable straight line, (curve E), that does not go through the origin.

Fig. 1 shows that the compliance values of the beam models are lower than the measured values for the same crack length. This comparison indicates that the beam length predicted by the simple beam model is longer than the crack length for the same compliance value. Fig. 1 also shows that by keeping the compliance value fixed and shifting curve (E) a distance $\Delta\ell$ to curve (S) then both curves will match each other almost perfectly. For any simulated crack length, ℓ, the compliance value is calculated from the simple beam equation in Fig. 1. For this compliance value, a corresponding beam length, $\ell_m = \ell_{model}$, of the built-in beam model can be obtained.

$$\ell = \ell_m - \Delta\ell \quad . \qquad (1)$$

$\Delta\ell$ depends on specimen geometry including the side-grooves and may depend on elastic moduli as well. Fig. 2 is a plot of ℓ versus ℓ_m from the measured compliance. The curve is fitted linearly to have a slope of 1 and the $\Delta\ell$ value is found to have an average value of 1.84 cm with at most -8%

deviation at the initial crack length and less than ±2% for $\ell > 8$ cm. Equation (1) is the calibration that relates the crack length to a simple beam crack model.

FRACTURE TEST DATA

A typical recorded fracture test data of the time varying shear force, Q(t), which is monitored by a 90° strain gage rosette, is shown in Fig. 3. A detailed description of this data has been reported in ref. [4]. Q(t) trace is digitized to form $Q(t)t^{1/2}$ which is proportional to the critical bending moment at the crack tip, M*. However, a smoothed $Q(t)t^{1/2}$ curve is used to calculate R(t) since the oscillations that appear on Q(t) and $Q(t)t^{1/2}$ are believed to be from stress waves producing complex beam vibrations. The numerically smoothed $Q(t)t^{1/2}$ curve is constructed from only three constants: the first gives the average K_{ID} values; the second specifies if K_{ID} increases or decreases with velocity and the last looks for a minimum in the curve. The smoothed $Q(t)t^{1/2}$ curve is used to provide: first, R(t), and thus $K_{ID}(t)$, as mentioned in the introduction; second, $\ell_m(t)$ by the built-in beam model [2,3,4]. $\ell_m(t)$ is corrected by equation (1) to provide an effective crack length $\ell(t)$. The derivative of $\ell(t)$ gives the crack propagation velocity, $\dot{\ell}(t)$. At each instant of time there is a K_{ID} and a corresponding $\dot{\ell}$ value. Thus, K_{ID} versus $\dot{\ell}$ from a single test can be obtained.

EXPERIMENTAL RESULTS

K_{ID} versus $\dot{\ell}$ curves are the final results from the rapid wedging dynamic fracture test. The test temperatures used in this study were -196°C, -140°C, -78°C, -60°C, -40°C and 0°C.

The fracture surfaces of the specimens tested at -196°C are reasonably

flat. In addition to the flat fracture there are only very small shear lips. The thickness of the specimen satisfies the static requirement for plane strain conditions. Thus, the dynamic stress intensity values are presumably plane strain. Fig. 4 shows the summary of these tests. K_{ID} decreases as $\dot{\ell}$ increases when $\dot{\ell}$ is below about 50 m/sec. K_{ID} reaches a minimum value versus $\dot{\ell}$ in the range of 50 m/sec to 80 m/sec. As $\dot{\ell}$ becomes higher than 80 m/sec, K_{ID} increases slightly as $\dot{\ell}$ increases. The upper three curves (i), (ii), (iii) show higher K_{ID} values at high $\dot{\ell}$ values. This may be due to a slight temperature gradient occuring throughout the specimen. The temperature close to the crack initiation end is slightly higher than the temperature at the far end of the specimen. The specimens from the two lower curves (iv), (v) have been very carefully temperature controlled to give a uniform temperature. The slightly increasing trend of K_{ID} vs $\dot{\ell}$ plot on the high $\dot{\ell}$ side may also be due to over estimating the resistance to fracture initiation because the starting crack, which is saw-cut, is not sharp enough - although it is dove tailed.

The fracture surface for -140°C test is reasonably flat and is similar to tests at -196°C. The starting crack on this specimen is also saw cut. K_{ID} vs $\dot{\ell}$ behaves the same as -196°C tests, see Fig. 5.

The fracture surface for the test at -78°C is flat for most part and appears rough near the very end of the specimen. A fatigue precrack is the starting crack. K_{ID} decreases monotonically as $\dot{\ell}$ increases in the tested $\dot{\ell}$ range as Fig. 6 shows. K_{ID} values from both curves (i) and (ii) have good reproducibility although $\dot{\ell}$ range changes quite a bit.

K_{ID} vs $\dot{\ell}$ for -60°C tests is shown in Fig. 7. All three specimens only broke half way down the beam. The fracture surfaces were still quite flat. Curve (i) of K_{ID} vs $\dot{\ell}$ shows a minimum around $\dot{\ell}$ = 50 m/sec. This

minimum may be mostly due to a temperature gradient (as mentioned early in this section) throughout the specimen, and partly due to the bluntness of the starting crack. Specimens for curves (ii) and (iii) have been carefully temperature controlled and have fatigued precracks. The low end $\dot{\ell}$ values may deviate quite a bit from the true $\dot{\ell}$, yet K_{ID} values show nice reproducibility.

Both specimens tested at -40°C and 0°C have fractured over 30 cm and then broke off. A fatigue precrack is used as the starting crack. The fracture path is quite flat at the beginning part and then turns rough in the later part of the specimen. In addition to the roughness of the fracture path there are a lot of broken ligaments on the fracture surfaces. These effects cause the crack to propagate quite slowly and K_{ID} is very high at low $\dot{\ell}$ values, see Fig. 8 and Fig. 9. Figure 10 is a plot of $Q(t)$ and $Q(t)t^{\frac{1}{2}}$ versus t for the 0°C specimen. The stress wave oscillations on $Qt^{\frac{1}{2}}$ are significantly smaller than the absolute change in the value of $Qt^{\frac{1}{2}}$ during the test. It follows that at higher temperatures that the rate dependence is a significantly stronger effect than the stress wave oscillations.

For all the specimens with either swallow tailed starting cracks or fatigue precrack the peak load K_{IC} values are higher than the K_{ID} values at the highest crack velocities. A typical example is shown in Fig. 3. K_{IC} corresponds to the first peak in the $Q(t)t^{\frac{1}{2}}$ trace. Physically, this point indicates the onset of fast fracture propagation as discussed in ref. 4 . K_{ID} is the corresponding point at the same time value on the smoothed $Q(t)t^{\frac{1}{2}}$ curve. The peak point is always higher, (higher value in $Qt^{\frac{1}{2}}$ scale), than the corresponding point on the smoothed curve. The higher $Qt^{\frac{1}{2}}$ value gives a higher stress intensity value. $\dot{K}$ values for all the K_{IC} tests reported varies from 1.2×10^5 to $5 \times 10^5 (MNm^{-3/2})/sec$.

CONCLUSIONS

Time varying shear force measurements have been applied to double cantilever beams specimens for studying dynamic crack propagation. This technique is based on the theory that the shear force across the loading end of a rapidly wedged slender DCB specimen times the square root of the loading time is proportional to the critical bending moment at the crack tip, M*. Static compliance measurements were used to incorporate the built-in beam model to the side-groove effects on the DCB specimen. The constant length shift correction will not affect the magnitude of M* and gives an effective crack length after correction. This correction is even valid for more sophisticated beam models [9,10] with side-grooves [4]. $Q(t)t^{\frac{1}{2}}$ is numerically smoothed to eliminate stress wave oscillations and this smoothed curve then provides the information for calculating $K_{ID}(t)$ and $\dot{\ell}(t)$. K_{ID} versus $\dot{\ell}$ has a generally decreasing trend as $\dot{\ell}$ increases and $|\partial K_{ID}/\partial \dot{\ell}|$ increases as temperature increases. For a single test $\dot{\ell}$ usually varies by a factor of 10.

This rapidly wedged DCB specimen test is unique in that the crack velocity starts at a high value and decreases throughout the test. The test has stability when K_Q at initiation is approximately the same value as K_{ID} and $\partial K_{ID}/\partial \dot{\ell}$ is negative. This keeps the crack's K value during the fracture event continually increasing. Crack propagation-arrest test specimens however seem to dominately test where $\partial K_{ID}/\partial \dot{\ell}$ is positive. Since, $\partial K_{ID}/\partial \dot{\ell}$ is negative in the low range of crack speeds, slow crack velocities are typical of the rapidly wedged DCB test. Occasionally a test specimen breaks an "arm" during testing. This phenomona is associated with the lack of stability of the fracture plane remaining on the symmetry plane of the slender DCB specimen. When the crack leaves the symmetry plane the K values tabulated are suspect. The reproducibility of the fracture tests is shown in the Experimental Results Section. For achieving good reproducibility, a stiff wedge,

a fatigued starting crack and a well controlled temperature environment are recommended. K_{IC} values at the onset of fast fracture propagation are also noted. These values are higher than the corresponding K_{ID} values for all the tests at different temperature for this low carbon steel.

Acknowledgements

This work was supported by the U.S. Department of Energy through contract EY-76-S-02-2422 at the University of Rochester.

References

1. C. Gurney and J. Hunt: Proc. Roy. Soc. (London), A299, 508, (1967).
2. Z.J. Bilek and S.J. Burns: J. Mech. Phys. Solids, 22, 85, (1974).
3. S.J. Burns and C.L. Chow: ASTM STP 627, 228, (1977).
4. C-Lun Chow and S.J. Burns: "Rapidly Wedged Crack Propagation Data with a Static Compliance Calibration", (to appear in International Journal of Fracture).
5. S.J. Burns: Air Force Materials Laboratory Technical Report AFML-TR-75-101, July (1975).
6. S.J. Burns: Proc. of 12th Annual Meeting of Society of Engineering Science, p. 121, (1975).
7. J.P. Berry: J. Appl. Phys., 34, 62, (1963).
8. R.G. Hoagland: J. Basic Eng., 89, 525, (1967).
9. M.F. Kanninen: Int. J. Fracture, 10, 415, (1974).
10. J.F. Malluck and W.W. King: Int. J. Fracture, 13, 655 (1977).

Figure Captions

Figure 1 Measured compliance values and beam model compliances versus crack lengths. Curve E is a fitted curve of measured values. Curve S is a Bernoulli-Euler beam on a rigid foundation with V shaped side-grooved cross section. Curve D is a dynamic Bernoulli-Euler beam on a rigid foundation with a V shaped side-grooved cross section.

Figure 2 The corresponding beam model crack length ℓ_m at a fixed compliance value versus the measured length, ℓ.

Figure 3 Scaled and smoothed $Q(t)$ and $Q(t)t^{\frac{1}{2}}$ traces for the test at -78°C. The peaks shown on $Q(t)$ are also shown on $Q(t)t^{\frac{1}{2}}$

Figure 4 K_{ID} versus $\dot{\ell}$ for a series of tests at -196°C.

Figure 5 K_{ID} versus $\dot{\ell}$ for the test at -140°C.

Figure 6 K_{ID} versus $\dot{\ell}$ for the tests at -78°C.

Figure 7 K_{ID} versus $\dot{\ell}$ for the tests at -60°C.

Figure 8 K_{ID} versus $\dot{\ell}$ for the test at -40°C.

Figure 9 K_{ID} versus $\dot{\ell}$ for the test at 0°C.

Figure 10 Scaled and smoothed $Q(t)$ and $Q(t)t^{\frac{1}{2}}$ traces for the test at 0°C. The rate effect is large since the value of $Q(t)t^{\frac{1}{2}}$ changes dramatically in the test.

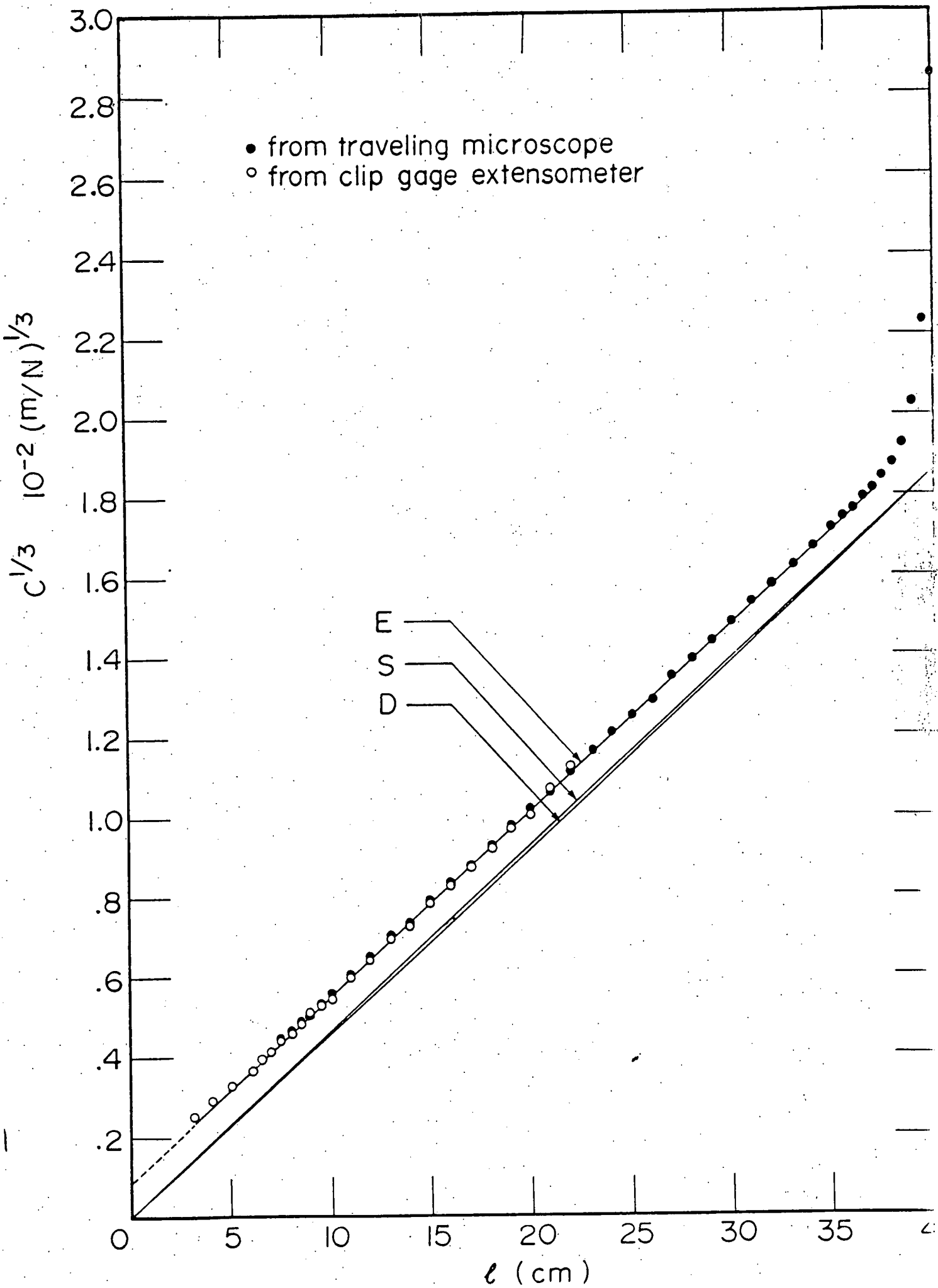
• from traveling microscope
° from clip gage extensometer
E
S
D
$C^{1/3}$ 10^{-2} $(m/N)^{1/3}$
3.0
2.8
2.6
2.4
2.2
2.0
1.8
1.6
1.4
1.2
1.0
.8
.6
.4
.2
0
5
10
15
20
25
30
35
ℓ (cm)

FIG 1

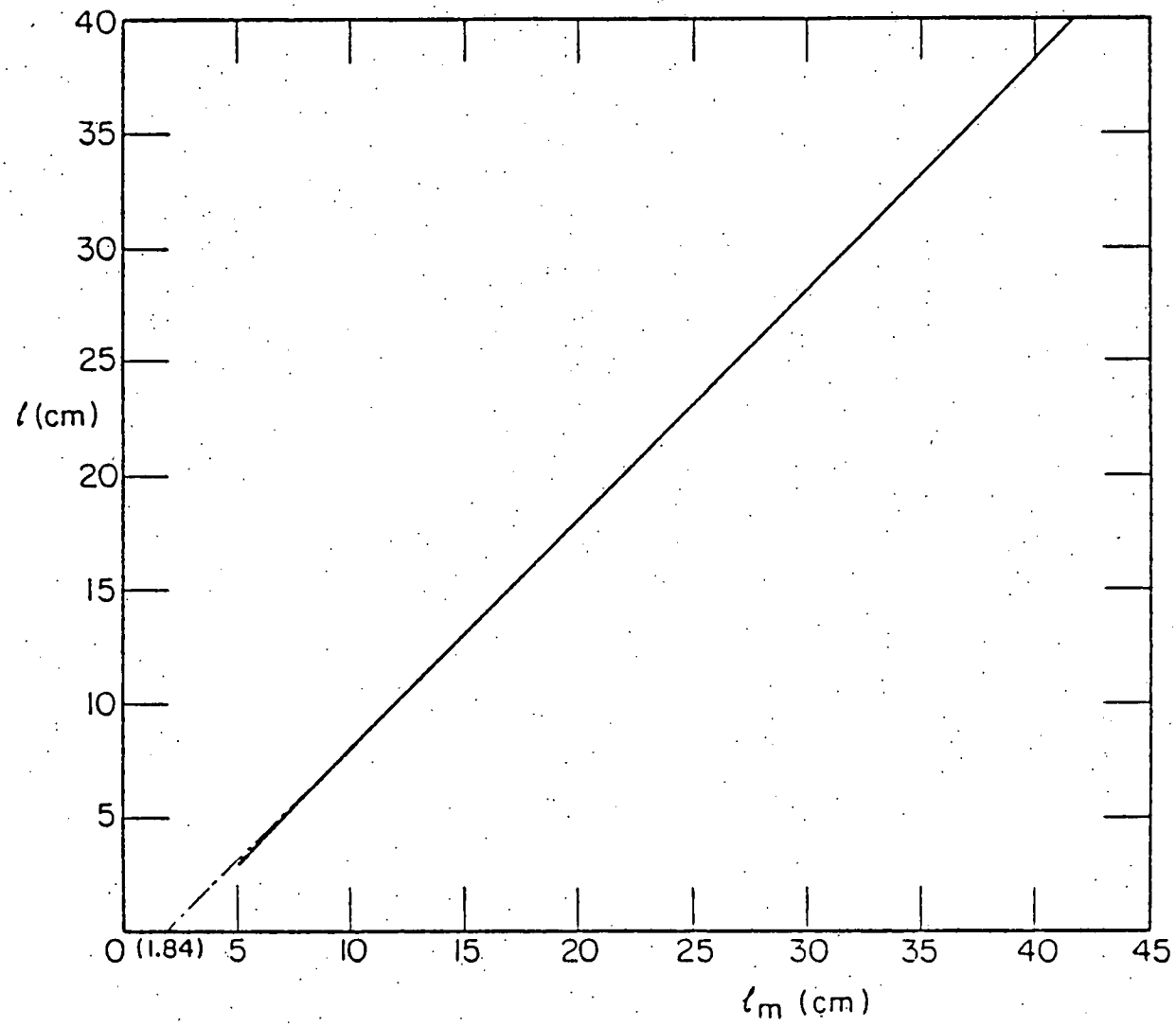

Fig. 2

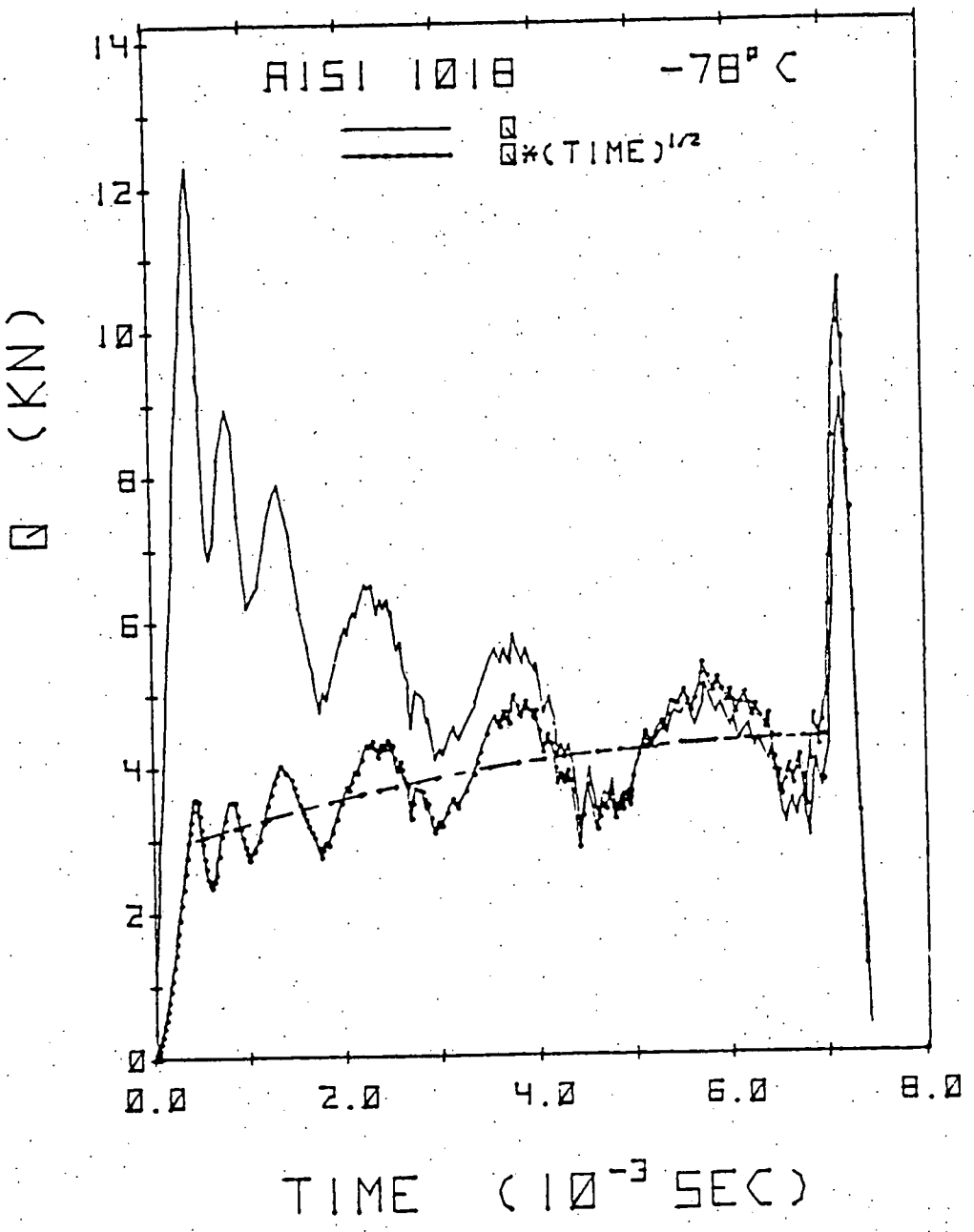
AISI 1018
-78° C
Q
Q*(TIME)^1/2
Q (KN)
Q*(TIME)^1/2
TIME (10^-3 SEC)
0
2
4
6
8
10
12
14
0.0
2.0
4.0
6.0
8.0

Fig 3.

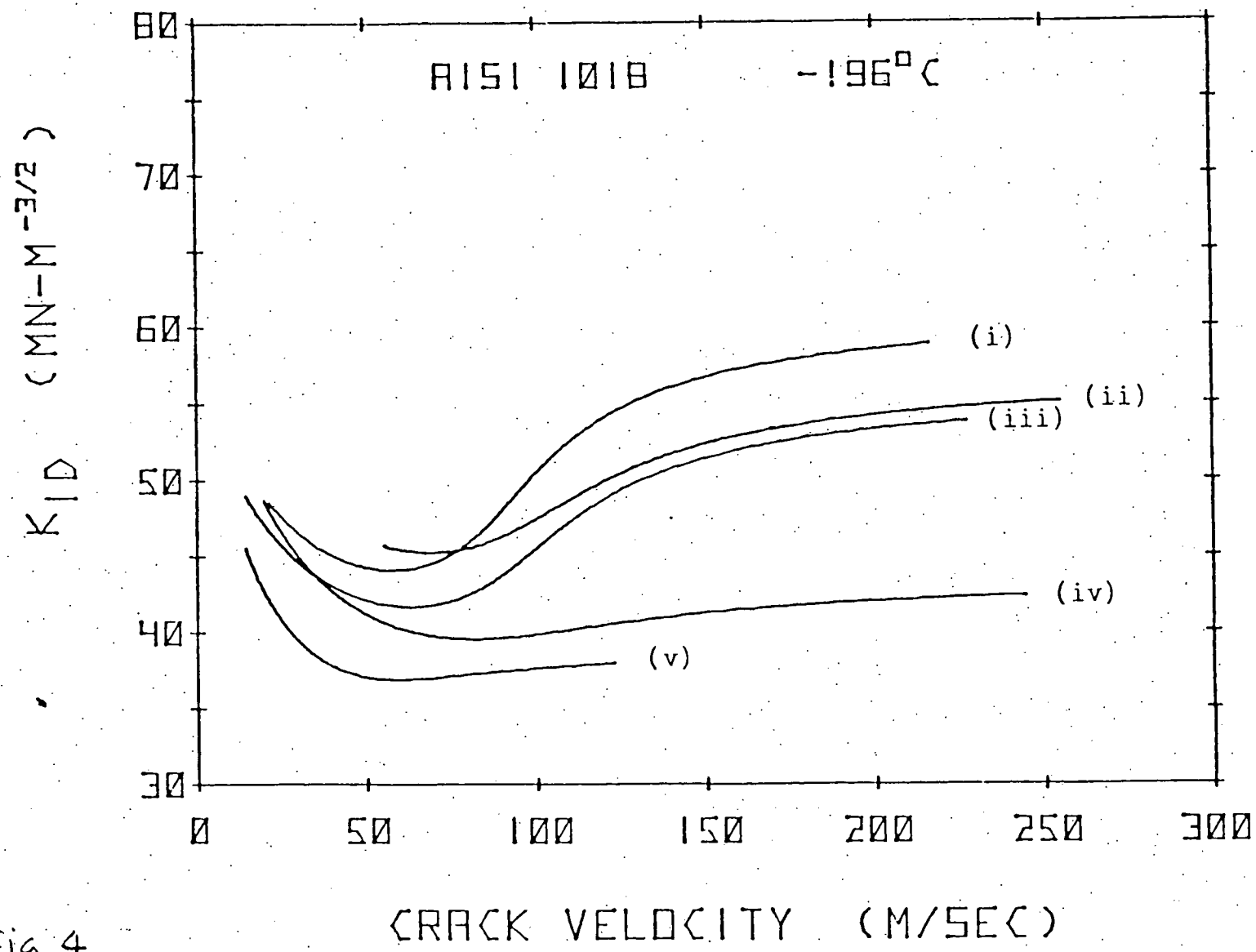
AISI 1018 -196°C
80
70
60
50
40
30
0
50
100
150
200
250
300
K_{ID} (MN-M$^{-3/2}$)
CRACK VELOCITY (M/SEC)
(i)
(ii)
(iii)
(iv)
(v)

Fig. 4

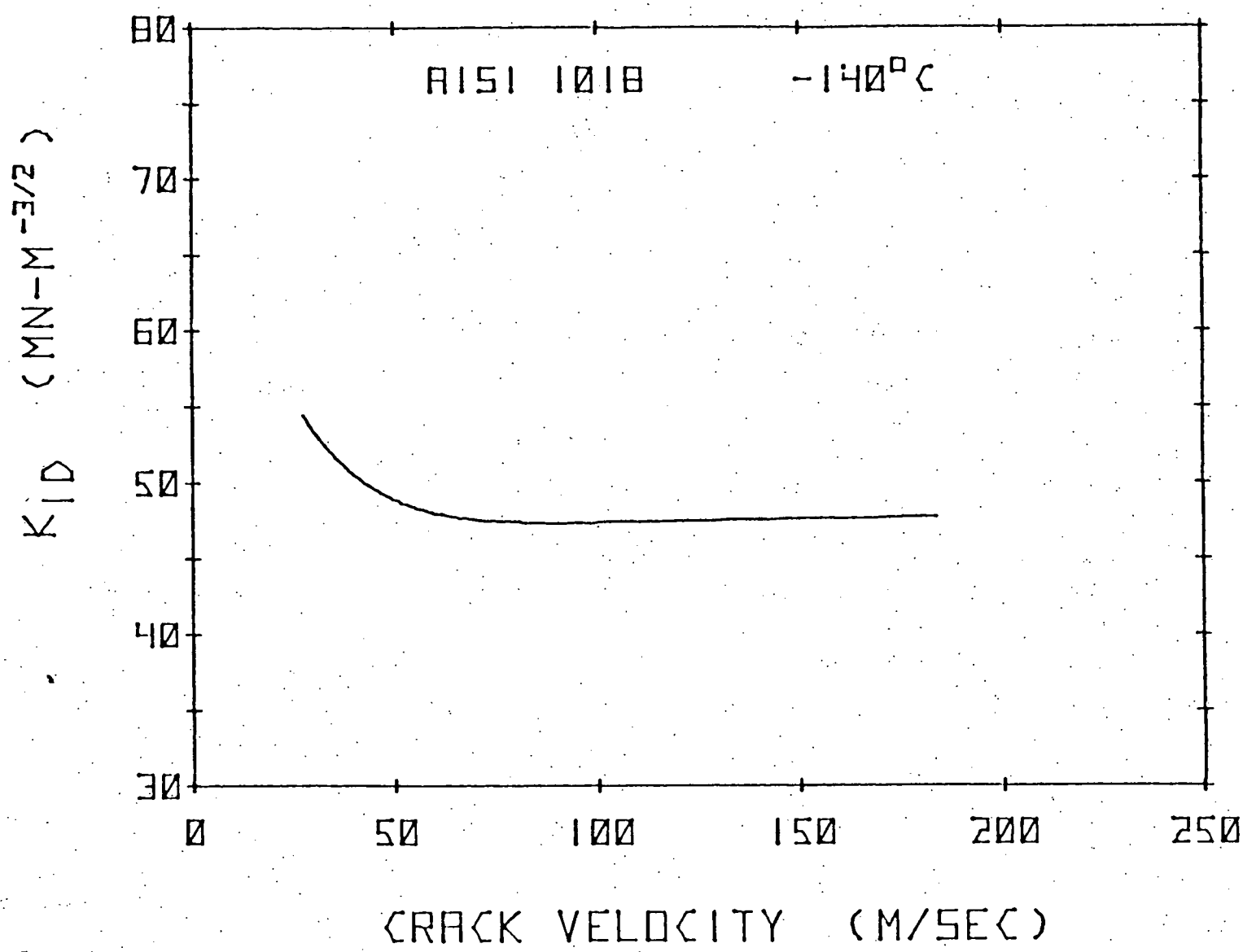
AISI 1018 -140°C
80
70
60
50
40
30
0
50
100
150
200
250
K_{ID} (MN-M$^{-3/2}$)
CRACK VELOCITY (M/SEC)

FIG 5

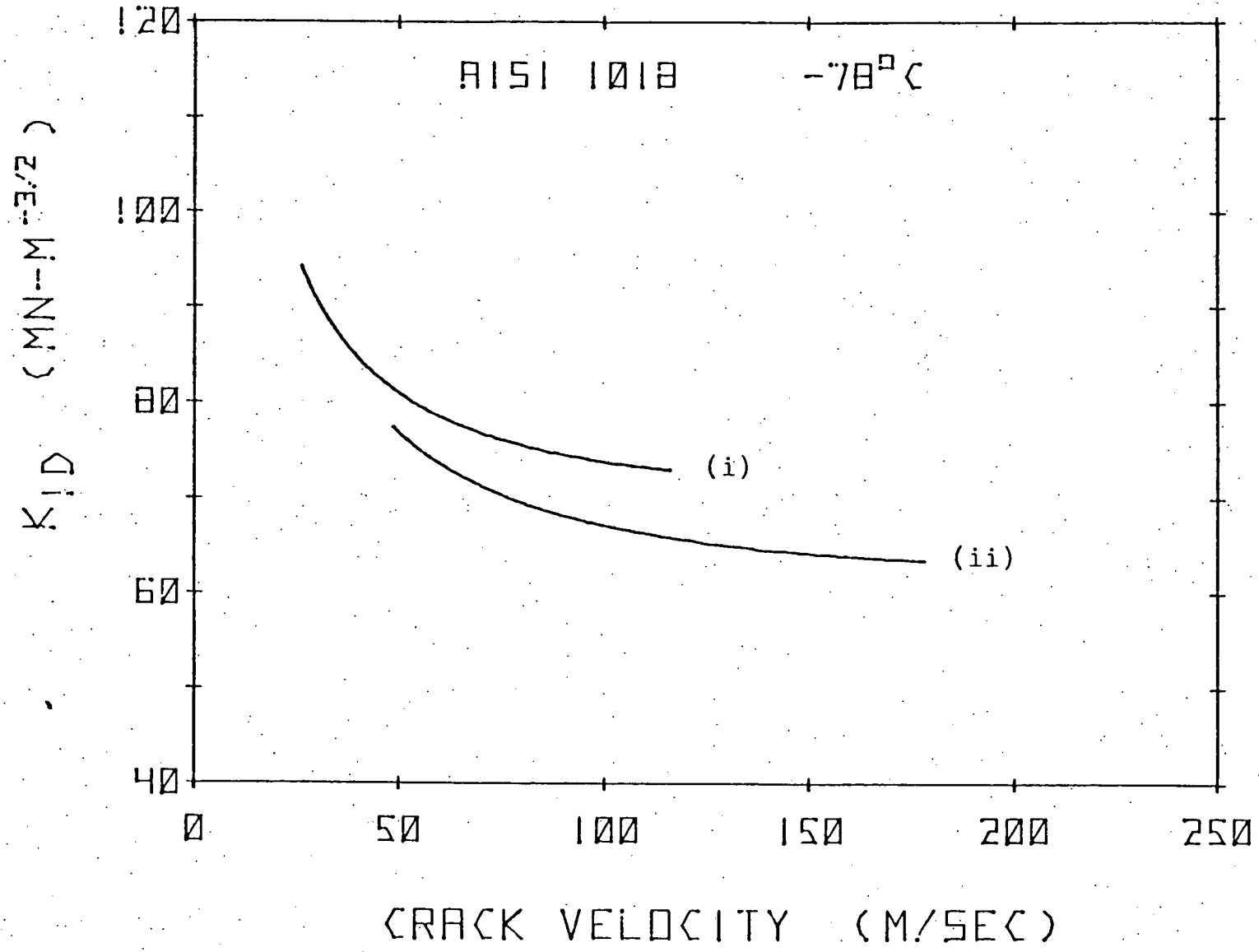
AISI 1018
-78°C
120
100
80
60
40
0
50
100
150
200
250
(i)
(ii)
K_{ID} (MN-M$^{-3/2}$)
CRACK VELOCITY (M/SEC)

Fig 6

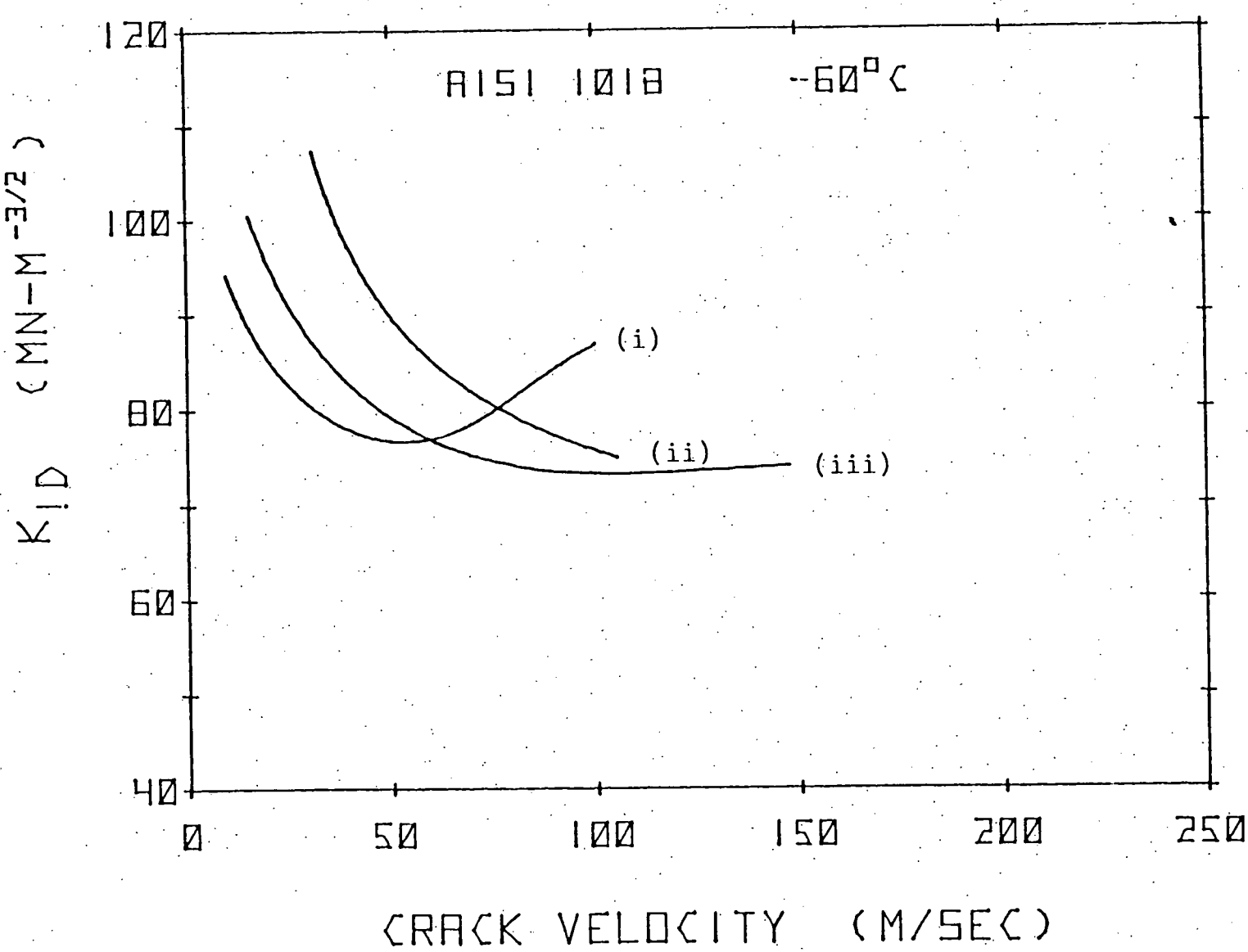
AISI 1018 --60°C
120
100
80
60
40
0
50
100
150
200
250
(i)
(ii)
(iii)
K_{ID} (MN-M$^{-3/2}$)
CRACK VELOCITY (M/SEC)

FIG 7

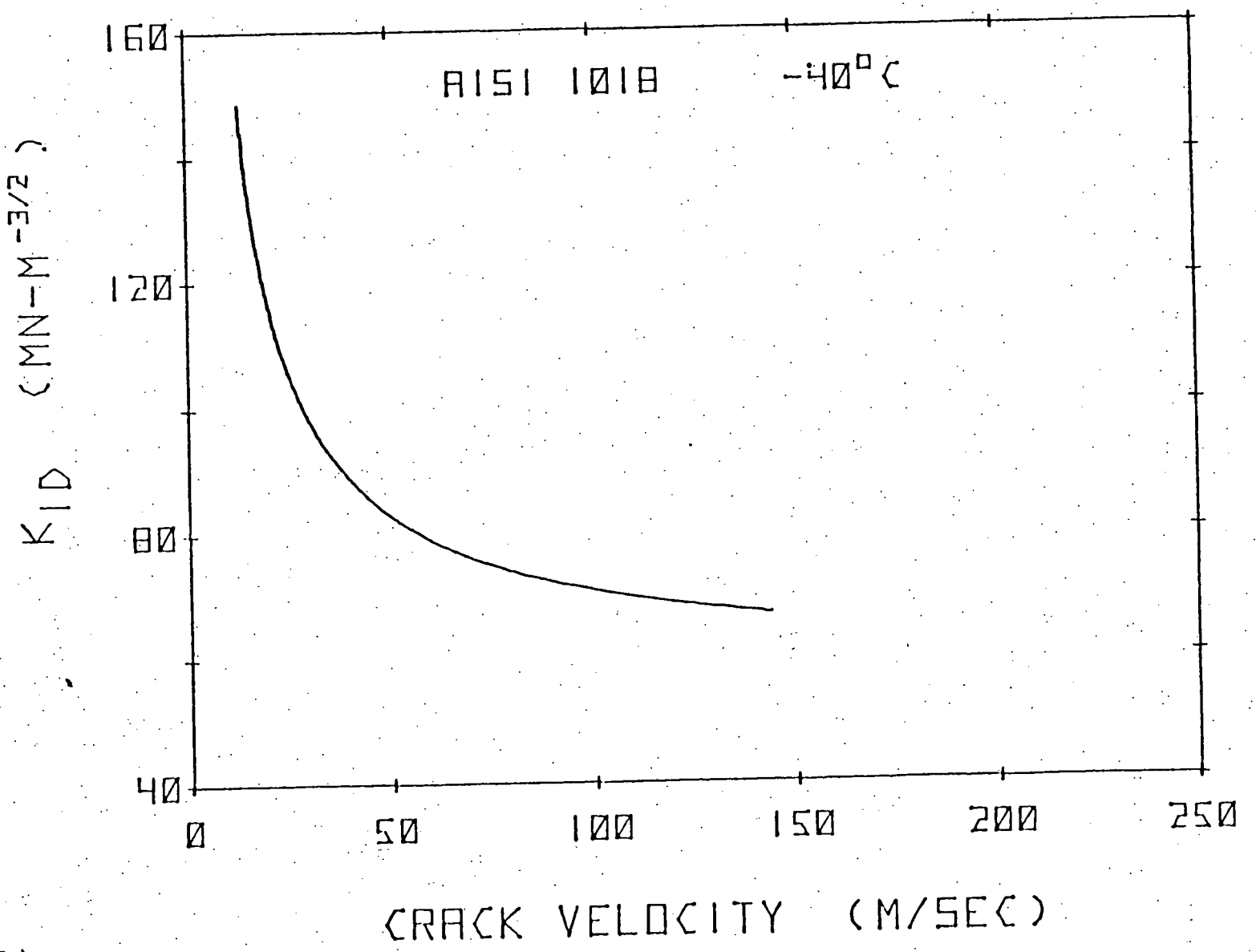
AISI 1018 -40°C
160
120
80
40
0
50
100
150
200
250
K_{ID} (MN-M$^{-3/2}$)
CRACK VELOCITY (M/SEC)

Fig 8

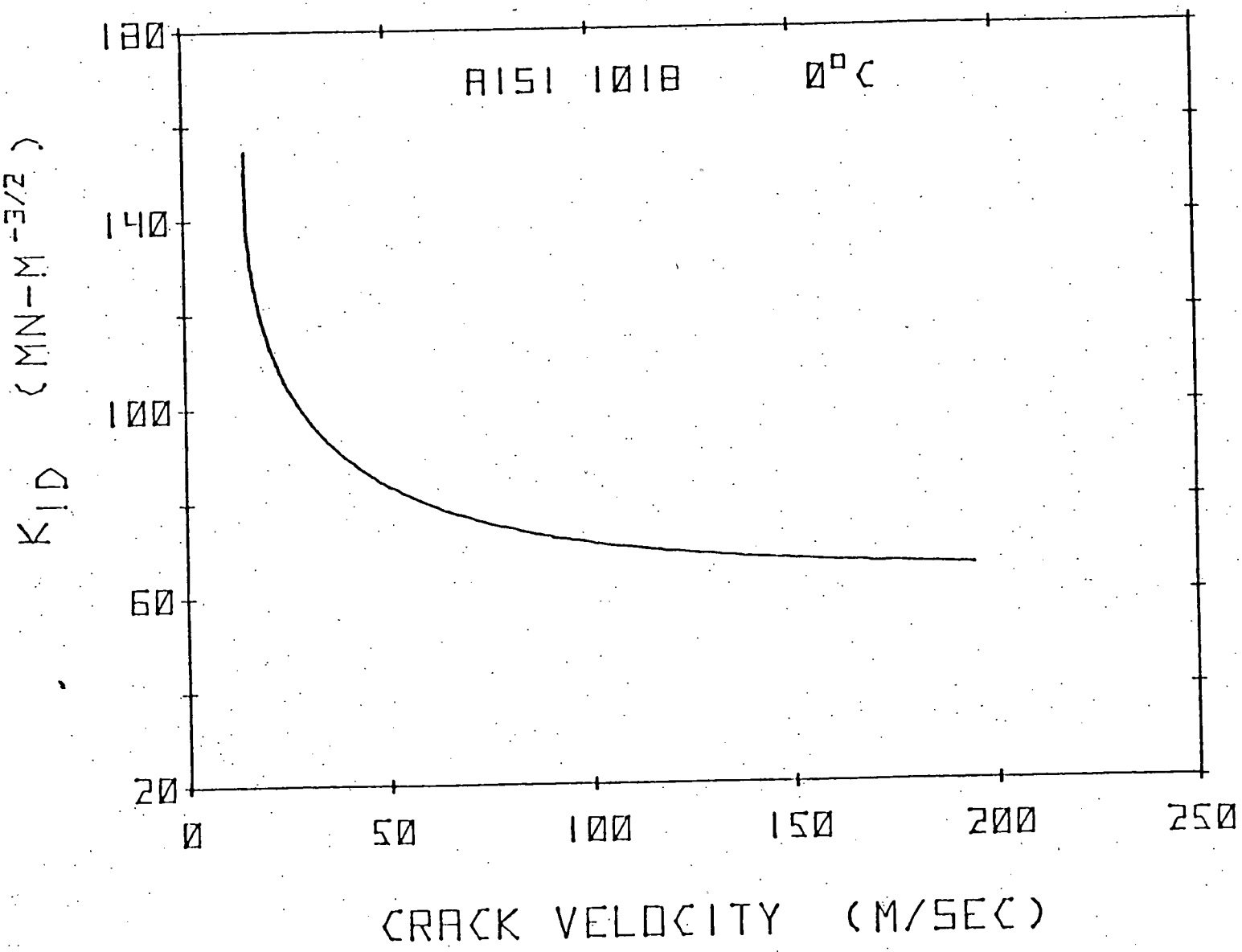
AISI 1018 0°C
180
140
100
60
20
K_{ID} (MN-M$^{-3/2}$)
0
50
100
150
200
250
CRACK VELOCITY (M/SEC)

Fig 9.

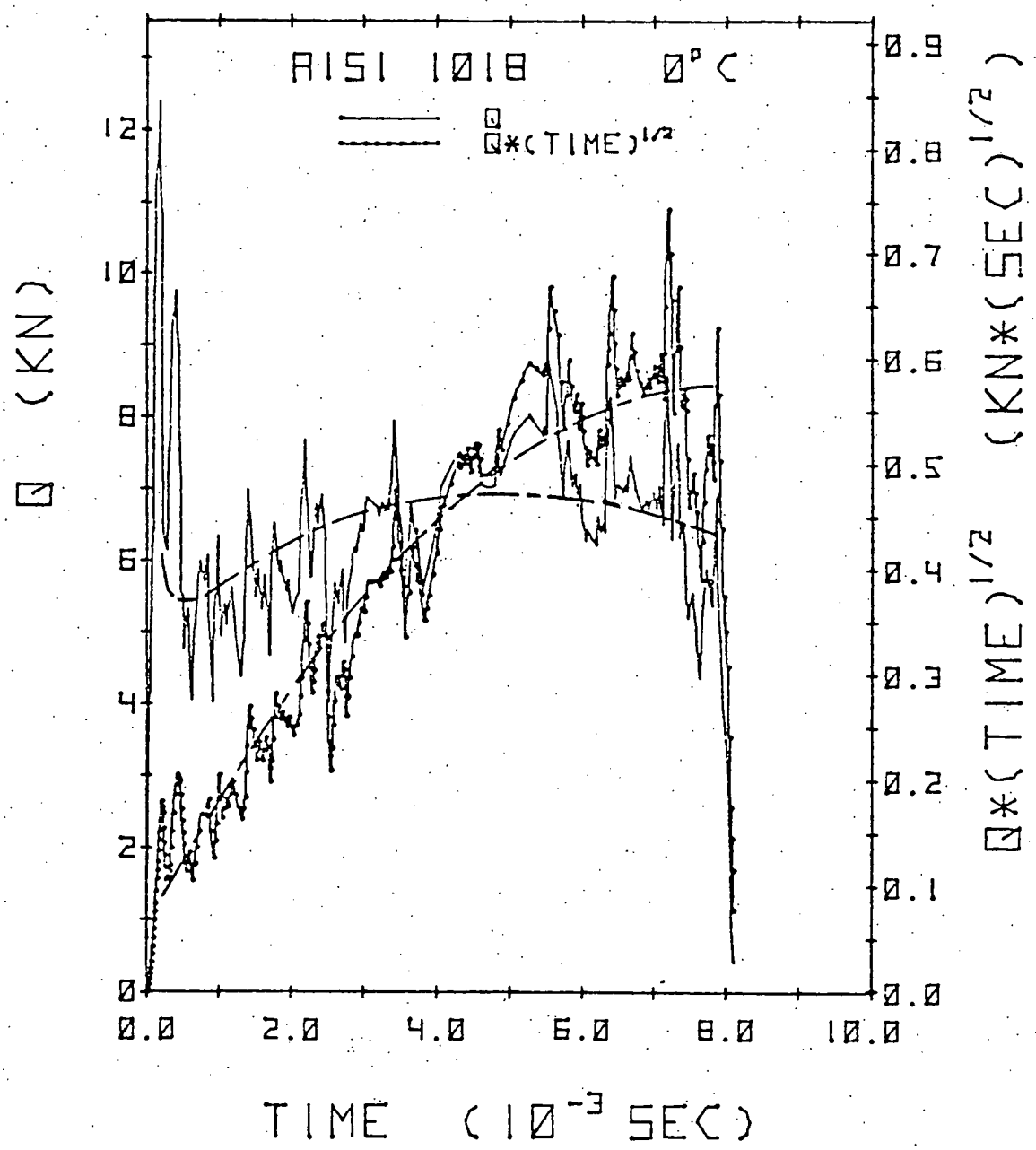
AISI 1018 0° C
Q
Q*(TIME)^1/2
Q (KN)
Q*(TIME)^1/2 (KN*(SEC)^1/2)
TIME (10^-3 SEC)
0
2
4
6
8
10
12
0.0
0.1
0.2
0.3
0.4
0.5
0.6
0.7
0.8
0.9
0.0
2.0
4.0
6.0
8.0
10.0

Fig 10